Electronic Research Archive

ERA, 31(3): 1570–1586.
DOI: 10.3934/era.2023080
Received: 21 November 2022
Revised: 27 December 2022
Accepted: 03 January 2023
Published: 31 January 2023

http://www.aimspress.com/journal/ERA

Research article

Improved active disturbance rejection controller for rotor system of magnetic levitation turbomachinery

Tongtong Yu, Zhizhou Zhang*, Yang Li, Weilong Zhao and Jinchu Zhang

School of Aeronautics and Astronautics, Sun Yat-sen University, Shenzhen 518107, China

* **Correspondence:** Email: zhangzhzh25@mail.sysu.edu.cn, zzz336@126.com.

Abstract: The rotor of the magnetic suspension turbomachinery is supported by the magnetic suspension bearing without contact and mechanical friction, which directly drives the high-efficiency fluid impeller. It has the advantages of high efficiency, low noise, less fault and no lubrication. However, the system often has some unknown mutation, time variation, load perturbation and other un-certainties when working, and the traditional Proportion Integration Differentiation (PID) control strategy has great limitations to overcome the above disturbances. Therefore, this paper firstly establishes a mathematical model of the rotor of magnetic levitation turbomachinery. Then, a linear active disturbance rejection controller (LADRC) is presented, which can not only improve the above problems of PID control, but also avoid the complex parameter tuning process of traditional nonlinear active disturbance rejection control (ADRC). However, LADRC is easy to induce the overshoot of the system and cannot filter the given signal. On this basis, an improved LADRC with a fast-tracking differentiator (FTD) is proposed to arrange the transition process of input signals. The simulation results show that compared with the traditional PID controller and single LADRC, the improved linear active disturbance rejection control method with fast tracking differentiator (FTD-LADRC) can better suppress some unknown abrupt changes, time variation and other uncertainties of the electromagnetic bearing-rotor system. At the same time, the overshoot of the system is smaller, and the parameters are easy to be set, which is convenient for engineering application.

Keywords: magnetic levitation turbomachinery; rotor system; tracking differentiator; improved LADRC; FTD-LADRC; anti-disturbance performance

1. Introduction

The magnetic levitation turbomachinery supports the rotor of the turbomachinery with magnetic levitation bearing, realizing the frictionless and wear-free support between the rotor of the turbomachinery and the stator, which can greatly improve the life and rotation speed of the turbomachinery [1]. However, due to the complexity of engineering application environment, unstable load, random disturbance and other problems, the stability analysis of magnetic bearing control system of magnetic levitation turbomachinery is very complicated, so it is significant to study the control algorithm of magnetic bearing system [2].

With the continuous development of control theory, many advanced control algorithms have been applied to the maglev system [3]. The robust control algorithm can keep the maglev system stable under uncertain factors, and avoid unknown interference and has a certain robustness, but it relies too much on the exact mathematical model of the controlled object [4]. The Linear Quadratic Regulator (LQR) method can generate complex control laws in the face of multi-variable systems, and solve problems such as multi-dimensional coupling and uncertainty interference, but the design of the controller needs to face the selection of two weighted matrices [5]. The Proportion Integration Differentiation (PID) control algorithm has the advantages of simple structure, clear physical meaning, easy implementation and good control effect under certain conditions, so it is widely used in maglev system. However, because the rotor system is often affected by external interference, it is difficult for PID to achieve high performance control [6].

On the basis of in-depth study of the advantages and disadvantages of PID control technology, Jingqing Han proposed an active disturbance rejection control technology (ADRC) [7]. This control technology does not depend on the object model, and can estimate and compensate the "internal disturbance" and "external disturbance" of the system in real time, with strong adaptability and anti-interference [8]. However, the nonlinear control structure is complicated and the adjustable control parameters are too many, so it is not easy to be applied quickly in engineering practice. Aiming at the shortcomings of the original nonlinear ADRC, Zhiqiang Gao proposed the concept of frequency scale, associated the parameters of ADRC in frequency domain, and proposed the linear active disturbance rejection controller (LADRC) [9]. LADRC linearizes the controller and the extended state observer, greatly reduces the adjustable parameters of the controller, and makes the active disturbance rejection control easier to applied to engineering. However, due to the cancellation of the tracking differentiator, the system is prone to overshoot. And when the input is polluted by noise, the input signal and differential signal cannot be extracted effectively [10].

Since maglev rotor system of turbomachinery is prone to position mutation, time variation and load perturbation, the active disturbance rejection control strategy is an effective scheme for interference suppression [11]. Because active disturbance rejection control not only requires less precision of modeling, but also can observe coupling disturbances among various degrees of freedom through extended state observer and implement compensation, so as to solve the decoupling and disturbance suppression problems in suspension control [12]. Therefore, the nonlinear model of the maglev turbomachinery rotor system is linearized at the equilibrium point, and the mathematical model is established. On this basis, by analyzing the advantages and disadvantages of ADRC and LADRC, an improved linear active disturbance rejection control method with fast tracking differentiator (FTD-LADRC) is proposed. In other words, the linear extended state observer (LESO) of LADRC is retained, and FTD is introduced to improve the complex structure of the tracking differentiator algorithm in

traditional ADRC. The algorithm can arrange the appropriate transition process according to the control target, reduce the overshoot caused by large changes, and at the same time can fast track the input signal of the system, and provide approximate differential signal. Finally, the simulation results show that the improved control algorithm has better anti-disturbance ability, fewer tunable parameters, and can realize the stable suspension of the rotor system.

2. Dynamic modelling of magnetic levitation rotor system

2.1. Working principle of magnetic levitation rotor system

The principle of maglev bearing-rotor system control is shown in Figure 1 [13]. The system consists of rotor, magnetic bearing, stator, power amplifier, eddy current sensor and controller. When the rotor is offset, the eddy current sensor will detect the deviation of the displacement in real time and feedback the displacement deviation signal to the controller [14]. The output signal of the controller forms a bias current through the power amplifier, which is sent to the electromagnet coil to form the electromagnetic force, so that the rotor returns to the balance position, so as to realize the active control of the electromagnetic bearing. The goal of the controller is not only to achieve the balance of electromagnetic force and rotor gravity, but also achieve the stability of the control loop [15,16].

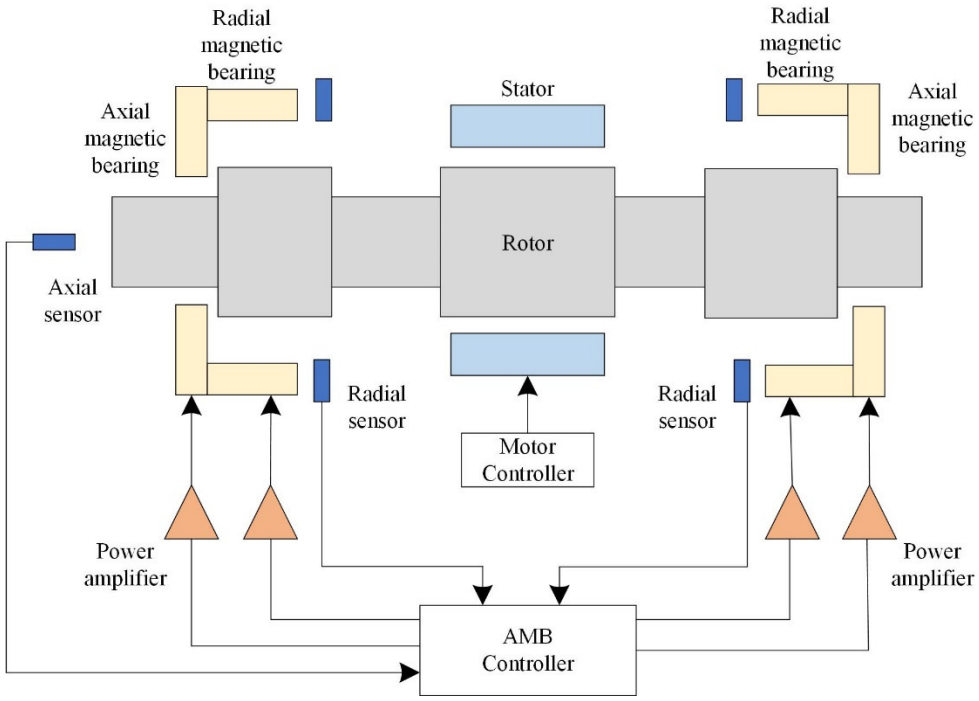

Figure 1. Structure of magnetic levitation bearing system.

As shown in Figure 1, it is the composition structure of the magnetic suspension bearing system. A pair of radial magnetic bearings are included to provide two translations of the rotor in the horizontal plane and two rotations of the shaft in space with four degrees of freedom, as well as two axial electromagnetic bearings to provide up and down motion of a Z-axis [17]. In these two cases, gyro effect coupling and inertial coupling can be forcibly ignored: 1) For inertial coupling, as long as the

rotor meets the requirement that its structure is completely symmetric, or the rotor is a slender rotor, then the inertial coupling can be coupled through the structure, making the coupling mass 0; 2) For gyroscopic effect coupling, when the rotor speed is below 60,000 rpm, the gyroscopic effect coupling can be ignored. Since the maglev rotor system used in this paper meets the conditions of mechanical decoupling and gyro effect decoupling, it can be simplified as a single-DOF system.

2.2. Mathematical model of a single-DOF rotor system

The eight-pole radial electromagnetic bearing as shown in Figure 2 is selected to study the relationship among magnetic force, displacement and current when moving in Y direction [18,19].

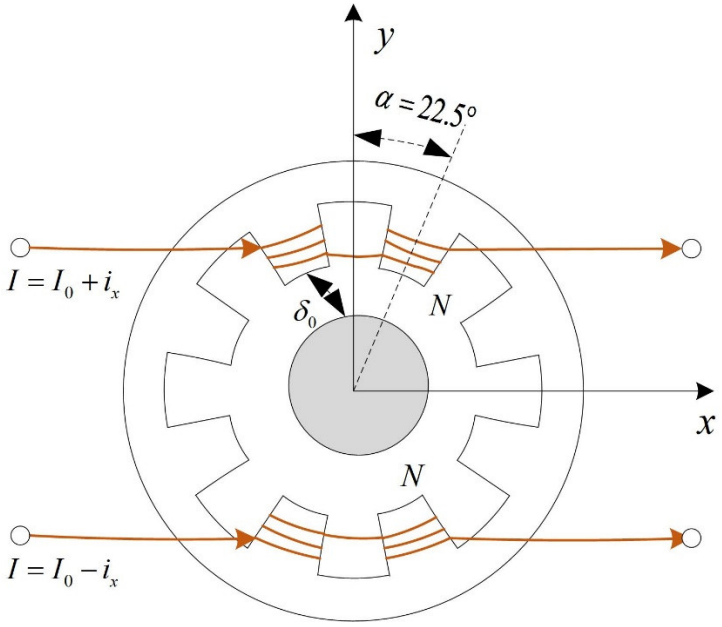

Figure 2. Schematic of single-DOF of eight-pole radial magnetic bearing.

1) Expression of electromagnetic force

The magnetic potential between the rotor surface and the electromagnet is considered to be uniformly distributed regardless of the magnetic resistance of the rotor and the core. At the same time, ignoring the magnetization of the electromagnet, the magnetic induction intensity between the stator and the rotor is calculated as follows [20]:

$$B = \frac{\mu_0 2NI}{2\delta_0} = \frac{\mu_0 NI}{\delta_0} \tag{1}$$

Where, μ_0 is vacuum permeability, I is current, δ_0 is air gap at equilibrium position, $2N$ is number of coil turns.

Based on Maxwell's electromagnetic attractive force formula:

$$f = \frac{B^2 A}{\mu_0} = \frac{\phi^2}{\mu_0 A} \tag{2}$$

Where, $\phi = BA$ is the magnetic flux, A is the sectional area of the electromagnet. By substituting

Eq (1) into Eq (2), the calculation formula of electromagnetic force can be obtained as follows:

$$f = k\frac{I^2}{\delta_0^2} \tag{3}$$

Where, $k = \mu_0 N^2 A$.

2) Linearization the electromagnetic force

The magnetic pole group model is shown in Figure 2, which is a differential control model in which the upper and lower forces jointly control the stable suspension of the rotor. The angle between the central axis of the stator and the center line of the electromagnet is defined as α. Ignoring the influence of the axial electromagnetic force, when the radial rotor has an offset x, the change of air gap in the Y-axis direction is $xcos\alpha$, and the air gap between the rotor and the upper and lower magnetic poles is $\delta_0 + x\cos\alpha$ and $\delta_0 - x\cos\alpha$. Then the controller outputs the control current to the upper and lower magnetic pole groups after receiving the signal. And i_x is the control current, I_0 is the equilibrium current. The current flowing through the upper magnetic pole coil is $I_0 - i_x$, and the current flowing through the lower magnetic pole coil is $I_0 + i_x$. Therefore, the electromagnetic forces generated by the upper and lower magnetic pole groups are respectively [21]:

$$f_{up} = \frac{1}{2}k\frac{(I_0 - i_x)^2}{(\delta_0 + x\cos\alpha)^2} \tag{4}$$

$$f_{down} = \frac{1}{2}k\frac{(I_0 + i_x)^2}{(\delta_0 - x\cos\alpha)^2} \tag{5}$$

Then, the electromagnetic resultant force in the y-direction is:

$$f_x = 2f_{down}\cos\alpha - 2f_{up}\cos\alpha = k\cos\alpha\left(\frac{(I_0 + i_x)^2}{(\delta_0 - x\cos\alpha)^2} - \frac{(I_0 - i_x)^2}{(\delta_0 + x\cos\alpha)^2}\right) \tag{6}$$

The equilibrium point is the point where the displacement is equal to 0 and the bias current is equal to 0 ($\triangle x = 0, i_x = 0$), near the equilibrium point the above equation is expanded by Taylor's theorem:

$$f_x(i_x, x) = f_x(i_{x0}, 0) + \frac{\partial f_x(i_{x0},0)}{\partial i}(i_x - i_{x0}) + \frac{\partial f_x(i_{x0},0)}{\partial x}x + \frac{1}{2!}\left[\frac{\partial^2 f_x(i_{x0},0)}{\partial i^2}(i_x - i_{x0})^2 + \frac{\partial^2 f_x(i_{x0},0)}{\partial i \partial x}(i_x - i_{x0})x + \frac{\partial^2 f_x(i_{x0},0)}{\partial x^2}x^2\right] + \cdots \tag{7}$$

Linear terms within the quadratic term are retained:

$$f_x(i_x, x) = f_x(i_{x0}, 0) + \frac{\partial f_x(i_{x0},0)}{\partial i}(i_x - i_{x0}) + \frac{\partial f_x(i_{x0},0)}{\partial x}x \tag{8}$$

By the Eq (3),

$$f_{x0} = f_x(i_{x0}, 0) = \frac{4kI_0 i_{x0}}{\delta_0^2}\cos\alpha \tag{9}$$

$$\left.\frac{\partial f_x}{\partial x}\right|_{(i_x = i_{x0}, x = 0)} = 4k\cos^2\alpha\frac{(I_0^2 + i_x^2)}{\delta_0^3} \tag{10}$$

$$\left.\frac{\partial f_x}{\partial i}\right|_{(i_x=i_{x0},x=0)} = 4k\cos\alpha\frac{I_0}{\delta_0^2} \tag{11}$$

Substituting Eqs (9)–(11) into Eq (8), the electromagnetic force at the equilibrium point can be linearized as:

$$f_x = 4k\cos^2\alpha\frac{I_0^2}{\delta_0^3}x + 4k\cos\alpha\frac{I_0}{\delta_0^2}i_x = k_x x + k_i i_x \tag{12}$$

where, $k_x = 4k\cos^2\alpha\frac{I_0^2}{\delta_0^3} = 4\mu_0 N^2 A\cos^2\alpha\frac{I_0^2}{\delta_0^3}$ is displacement stiffness coefficient, $k_i = 4k\cos\alpha\frac{I_0}{\delta_0^2} = 4\mu_0 N^2 A\cos\alpha\frac{I_0}{\delta_0^2}$ is current stiffness coefficient.

3) Transfer function of electromagnetic bearing system

The dynamic equation of the rotor in radial direction is listed as follows:

$$m\frac{d^2x}{dt} = f_x + mg \tag{13}$$

Substituting the electromagnetic force Laplace transform Eq (12) for Eq (13):

$$ms^2X(s) = k_x X(s) + k_i I(s) \tag{14}$$

Finally, the transfer function between rotor offset and control current is obtained:

$$G_m(s) = \frac{X(s)}{I(s)} = \frac{k_i}{ms^2 - k_x} \tag{15}$$

Because the transfer function $G(s)$ has an unstable pole, the system is unstable. Therefore, it is necessary to design a controller to make the closed-loop rotor system stable. The magnetic bearing control system is shown in Figure 3.

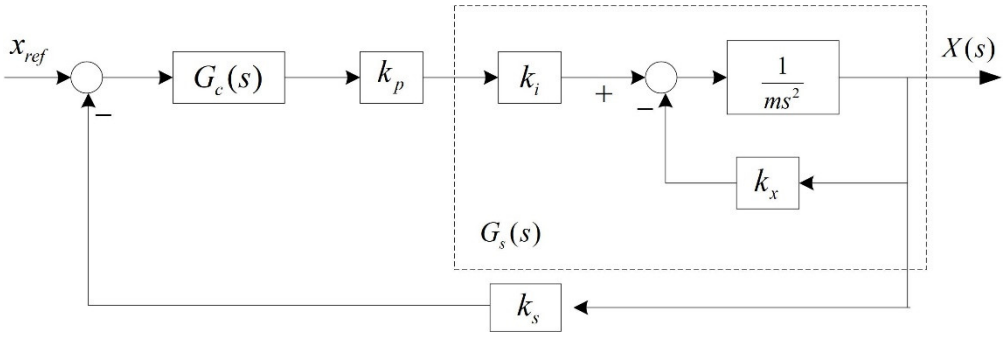

Figure 3. Magnetic bearing control system diagram.

As can be seen from Figure 3, the expression of current transfer function is $I(s) = k_c G_s(s) G_c(s) X(s)$, The transfer function of the complete closed-loop electromagnetic bearing system is $G(s) = \frac{k_s k_p G_c(s)}{1 + k_s k_p G_c(s) G_s(s)}$.

Here, $G_c(s)$ is the transmission function of the controller, k_p and k_s are the gain of the power amplifier and sensor respectively, k_i, k_x are the current stiffness coefficient and displacement

stiffness coefficient, respectively.

According to the practical requirements, different controllers $G_c(s)$ can be selected. This paper mainly studies PID controller and active disturbance rejection controller.

3. Design of FTD-LADRC

3.1. Overall framework of FTD-LADRC

The LADRC structure is shown in Figure 4. It is mainly composed of a linear extended state observer and a linear control law. Compared with LADRC, the improved LADRC (Figure 5) adds a FTD and makes some improvements in the control law. When the rotor of magnetic bearing is offset, it is the input signal of given displacement, and FTD arranges the appropriate transition process for the given signal to get the tracking signal and differential signal. The linear extended state observer can not only observe the original state variables of the system, but also expand the total disturbance into a new state variable. Then the error of the two is used to calculate the control quantity according to a certain linear feedback law, which is applied to the rotor to restore the rotor to the equilibrium position [22].

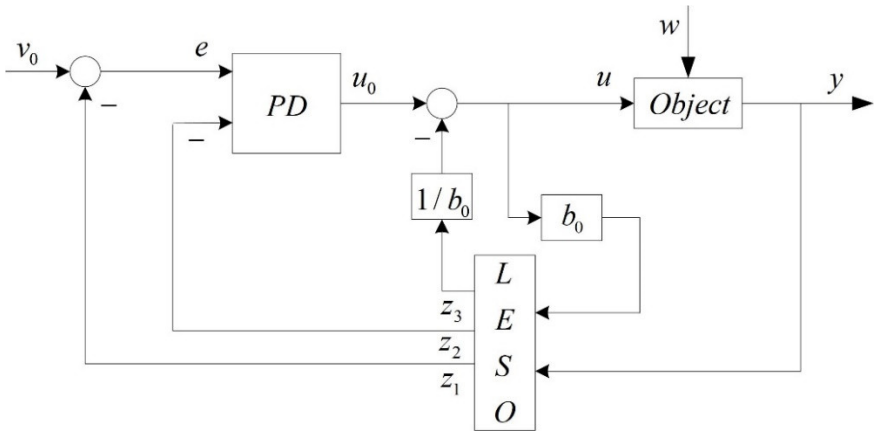

Figure 4. General linear active disturbance rejection controller.

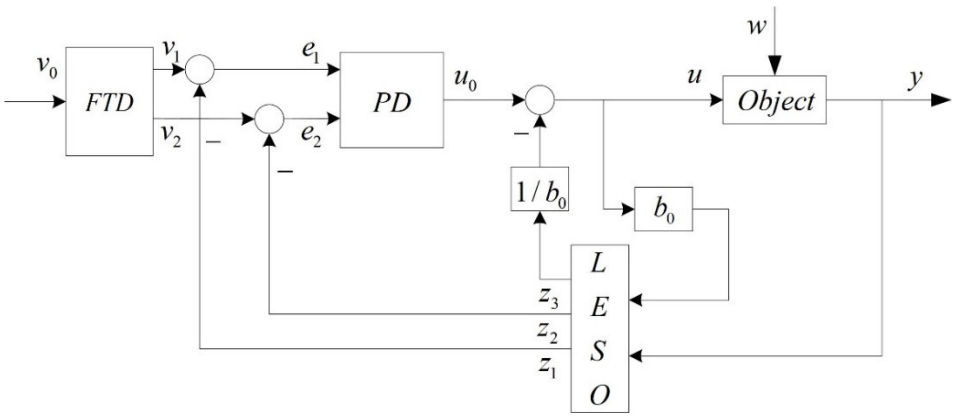

Figure 5. Improved linear active disturbance rejection controller with FTD.

Now, we establish the standard formula of the second-order controlled object: $\ddot{y} = f(y, \dot{y}, w, t) + bu$, where, y,u are output and input respectively; w is external disturbance; b is a parameter; $f(y, \dot{y}, w, t)$ is the total disturbance.

3.2. Fast tracking differentiator (FTD)

In general control systems, the error is directly taken as the difference between the system output and the set value. This method makes the initial value of the error very large, which is easy to cause overshoot. If a reasonable transition process is first arranged and the error is taken as the difference between the transition process and the output value, the contradiction between "speediness" and "overshoot" can be solved.

Jingqing Han proposed the concept of nonlinear tracking differentiator [23], its discrete tracking differentiator has the following form:

$$\begin{cases} x_1(k+1) = x_1(k) + hx_2(k), \\ x_2(k+1) = x_2(k) + hfst(x_1(k) - v, x_2(k), r, h_0). \end{cases} \tag{16}$$

Where,

$$fst(x_1 - v, x_2, r, h_0) = \begin{cases} -ra, |a| \le d; \\ -rsign(a), |a| > d. \end{cases}$$

$$a = \begin{cases} x_2 + \frac{c}{h_0}, |c| < d_0; \\ x_2 + \frac{sign(c)(a_0 - d)}{2}, |c| > d_0. \end{cases} \tag{17}$$

$$\begin{aligned} d &= rh_0, \\ d_0 &= dh_0, \\ c &= v_1 - v + h_0 v_2, \\ a &= \sqrt{d^2 + 8r|c|}. \end{aligned}$$

Where, v is the input signal, x_1 is the tracking signal of v, x_2 is the derivative of x_1, namely, the differential signal of v; h is the integral step, r determines the tracking speed, h_0 determines the noise filtering effect, r and h_0 needs to be coordinated and adjusted to obtain satisfactory performance.

Its discrete form can eliminate chatter and has good performance. But it uses two switching functions, the algorithm form is complex, the controller calculation is large, the system hardware requirements are high, and not easy to engineering application.

Literature [10] puts forward an improved tracking differentiator, whose form is as follows:

If $R > 0, \alpha_1 > 0, \alpha_2 > 0, \beta$ is a constant greater than or equal to 1, $p > q > 0$, p and q are both odd, then for any input signal $v(t) \in L \in [0, \infty)$ and any constant $T > 0$, we can get the system

$$\begin{cases} \dot{x}_1 = x_2, \\ \dot{x}_2 = -\alpha_1 R^2 \left[(\beta(x_1 - v))^{p/q} + x_1 - v \right] - \alpha_2 R^2 \left[(\beta x_2 / R)^{p/q} + x_2 / R \right] \end{cases} \tag{18}$$

and the solution to the formula satisfies: $\lim_{R \to \infty} \int_0^T |x_1(t) - v(t)| \, dt = 0$.

When the tracking error is large, the tracking differentiator adopts nonlinear link to accelerate the

speed of approaching the equilibrium point. When the error is small, the linear link is used to avoid flutter. The tracking differentiator has good dynamic response and strong filtering ability, and can track and differentiate arbitrary signals.

3.3. Linear extended state observer (LESO)

The basic idea of LESO is to expand the total disturbance into a new state variable of the system, and then observe all the states including the original state variables and disturbances of the new system by using the system input [24].

Here $x_1 = y, x_2 = \dot{y}$ are the state variables, the total disturbance f is the augmented variable x_3, that is $x_3 = f = h$, its state space expression is:

$$\begin{cases} \dot{x} = Ax + Bu + Eh, \\ y = Cx, \end{cases} \tag{19}$$

Where, $x = (x_1, x_2, x_3)^T, A = \begin{bmatrix} 0 & 1 & 0 \\ 0 & 0 & 1 \\ 0 & 0 & 0 \end{bmatrix}, B = (0, b_0, 0)^T, E = (0,0,1)^T, C = [1,0,0]$.

The three-dimensional expanded state observers are:

$$ESO: \begin{cases} \dot{z} = Az + Bu + L(y - \hat{y}), \\ \hat{y} = Cz, \end{cases} \tag{20}$$

Where, $z = (z_1, z_2, z_3)^T$ is the state variable of ESO; $L = (\alpha_1, \alpha_2, \alpha_3)^T$ is the observer gain of ESO. If all the poles of the observer are configured at ω_o, $det\big(sI - (A - LC)\big) = s^3 + \alpha_1 s^2 + \alpha_2 s + \alpha_3 = (s + \omega_o)^3$.

Therefore $\alpha_1 = 3\omega_o, \alpha_2 = 3\omega_o^2, \alpha_3 = \omega_o^3$.Thus, the observer can be written as

$$ESO: \dot{z} = (A - LC)z + Bu + Ly \tag{21}$$

Plug in the parameters, it can get $\dot{z} = \begin{bmatrix} -\alpha_1 & 1 & 0 \\ -\alpha_2 & 0 & 1 \\ -\alpha_3 & 0 & 0 \end{bmatrix} z + \begin{bmatrix} 0 & \alpha_1 \\ b_0 & \alpha_2 \\ 0 & \alpha_3 \end{bmatrix} \begin{bmatrix} u \\ y \end{bmatrix}$.

3.4. Linear control combination

The nonlinear error feedback control law in ADRC is linearized, and the classical PID combination is used to implement the controller design. Since the ESO can estimate and compensate external and internal disturbances in real time, it is further simplified to a linear control combination. Due to the addition of tracking differentiator to the signal input, the control law here has some improvement compared with LADRC [25].

$$u_0 = k_1(v_1 - z_1) + k_2(v_2 - z_2) \tag{22}$$

where, v_1 and v_2 are the tracking signal and differential signal of the tracking differentiator, z_1 and z_2 are the observer states from LESO, k_1 and k_2 are the amplification coefficients of proportion (P) and differential (D) respectively.

3.5. Disturbance compensation calculation

When the rotor of the actual magnetic suspension bearing is in stable suspension, it may encounter load mutation, interference of a certain frequency and external force impact, and may also have noise signals on the spot introduced into the displacement signal. These disturbances will have a certain impact on the control [26].

Through LESO, the representative disturbance state variable x_3 expanded from the original system is tracked by z_3 in the extended state observer. The disturbance is compensated by the control quantity, which is transformed into an integral series control problem. The control quantity is obtained as:

$$u = \frac{u_0 - z_3}{b_0} \tag{23}$$

Where, $-\frac{z_3}{b_0}$ is the component that compensates the disturbance, and $\frac{u_0}{b_0}$ is the component that uses linear feedback to control the series type of integrator.

4. Controller tuning and simulation analysis

After linearization, there are $R, \alpha_1, \alpha_2, \beta, p, q, k_1, k_2, b, \omega_o$ ten parameters in the FTD-LADRC part. But the controller tuning has a certain rule, and the controller has strong robustness, and it is easy to adjust parameters. The parameter b is the only parameter related to the system. It can be assumed to be an approximate estimation constant value b_0 during simulation. According to the mathematical model of the magnetic suspension bearing system, get the value of b.

The setting method of ω_o is the same as that of LADRC. The k_1 and k_2 in the control law can be adjusted from large to small by trial and error, and then the parameters can be adjusted according to the running condition of the controlled object.

For the FTD, reference [10] shows that there are six parameters $R, \alpha_1, \alpha_2, \beta, p, q$ to be adjusted. Through simulation, it is found that the value of some parameters is relatively fixed, which has little influence on the simulation results, so the workload of parameter adjustment is also small.

The magnetic levitation bearing of the controlled object uses the parameters in Table 1 below.

Table 1. The system parameters of magnetic bearing.

Parameters	Symbol	Values
The quality of rotor	m	$2.349\ kg$
Magnetic pole coil turns	N	120
Magnetic pole cross-sectional area	A	$200\ mm^2$
Nominal air gap	δ_0	$0.4\ mm$
Permeability of vacuum	μ_0	$4\pi e * 10^{-7}\ Vs/Am$
Bias current	I	$1.1\ A$
Power amplifier gain	k_p	$0.22\ A/V$
Sensor gain	k_s	$20{,}000\ V/m$
Current stiffness	k_i	$91.95\ N/A$
Displacement stiffness	k_x	$233{,}614\ N/m$

Meanwhile, the open-loop transfer function of the electromagnetic bearing system is obtained as follows:

$$G_m(s) = \frac{Y(s)}{I(s)} = \frac{91.95}{2.349s^2 - 233614} \tag{24}$$

1) The output performance of FTD

The model parameters of two kinds of tracking differentiators are shown in Table 2. In order to verify the tracking characteristics of the tracking differentiator, sinusoidal signals are fed into the input in Figure 6. It can be seen that the FTD algorithm has faster dynamic characteristics. The phase lag problem has been improved.

Table 2. The model parameters of TD and FTD.

Parameters	Values	Parameters	Values
r	9000	α_2	2
c_0	2	β	1
R	300	p	9
α_1	2	q	3

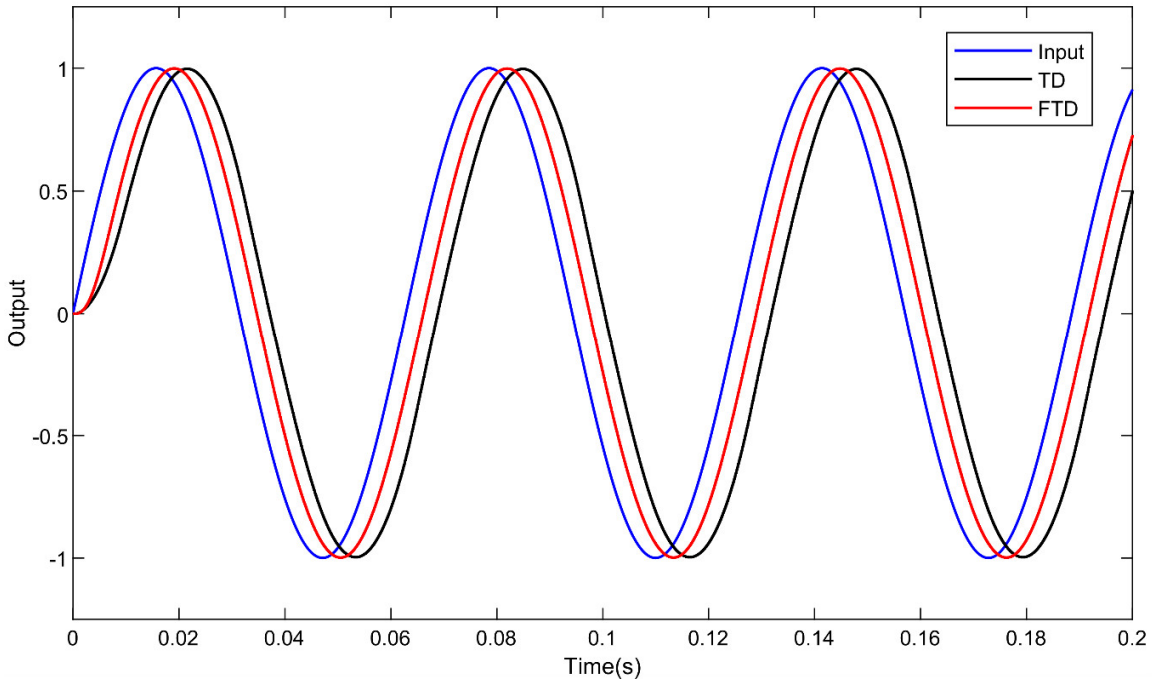

Figure 6. Comparison of simulation results of tracking differentiator without interference.

In order to verify the filtering effect of the two tracking differentiators, a constant value of 0 is fed into the input, and a Gaussian white noise with mean value of 0 and mean square deviation of 0.003 is added. As can be seen from Figure 7, both tracking differentiators have filtering effects, but the filtering effect of high-frequency noise using FTD is more significant. At the same time, FTD algorithm form is simple, and there is no complex switch function.

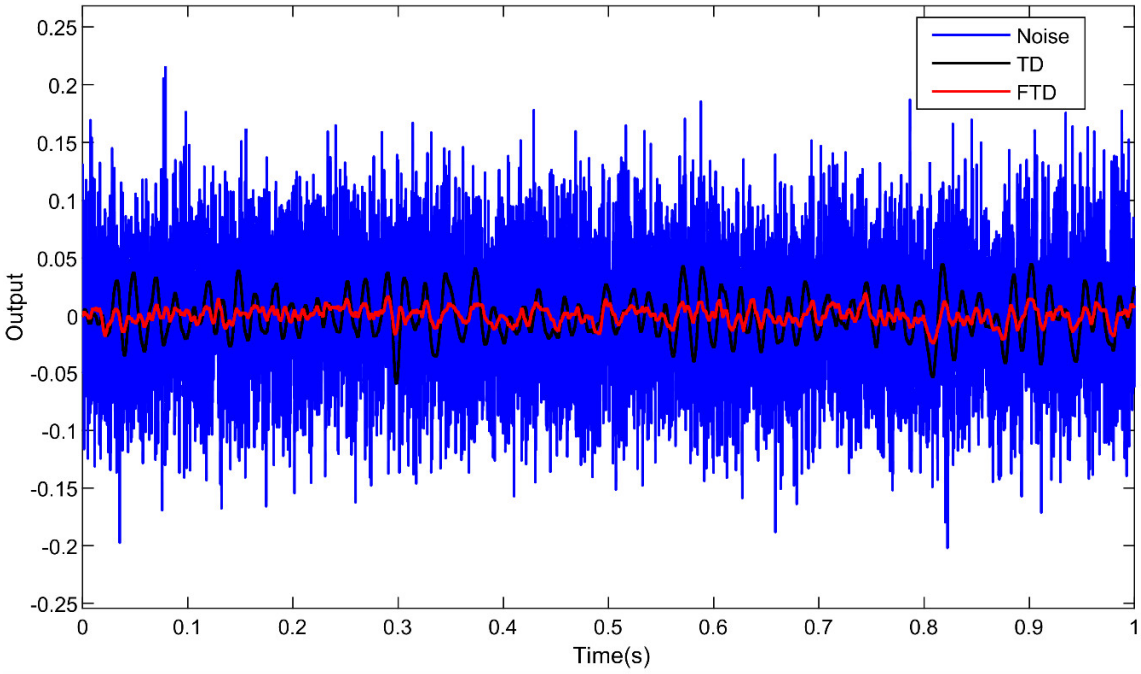

Figure 7. Comparison of simulation results of tracking differentiator with noise.

2) Rotor offset case

The system is assumed to have a 0.2mm displacement offset, namely a unit step signal, is assigned to the system input, and three controllers (PID, LADRC, FTD-LADRC) are used to model the maglev bearing control system. The parameters of the FTD-LADRC controller are shown in Table 3.

Table 3. Parameters of FTD-LADRC controller.

Parameters	Values	Parameters	Values
k_1	4,000,000	α_2	6
k_2	140,000	β	1
b	404,580	p	9
R	150	q	3
α_1	6	ω_o	70,000

The simulation curves of the three controllers verified under step response are shown in Figure 8. The overshoot of the unit step response curve controlled by PID is 20%, the rise time is 0.025 s, and the adjustment time is 0.075 s. Observing the step curves in the figure, it can be found that LADRC and FTD-LADRC are significantly more superior than PID control in terms of overshoot and steady-state time, entering the steady state at 0.04 s. However, in the process of parameter adjustment, it is found that when the parameters of LADRC are not suitable, it is easier to overshoot than FTD-LADRC, and FTD-LADRC has good robustness. For example, when the value of ω_o of LADRC is not suitable and changed to 7000, the system experiences an overshoot as shown in Figure 9.

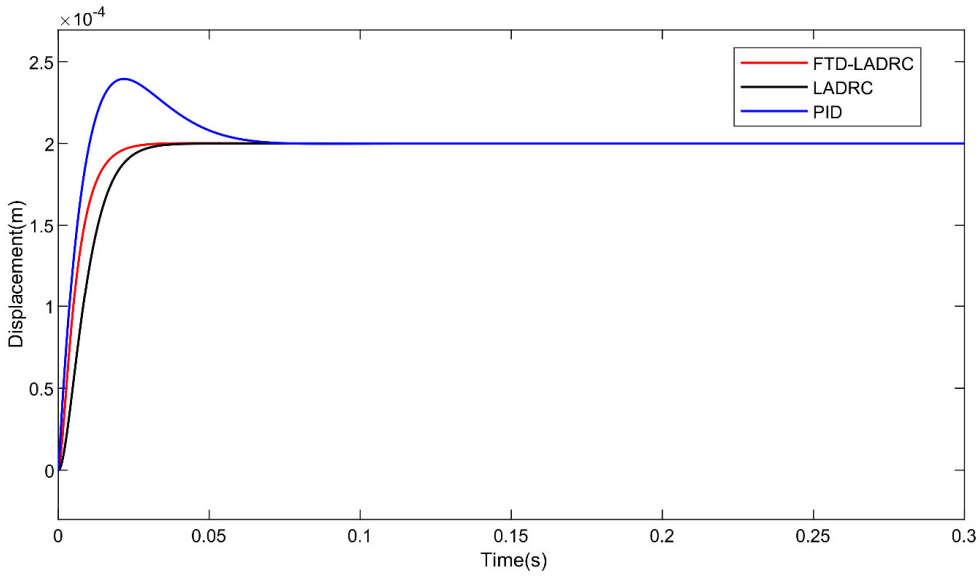

Figure 8. Step response curves of magnetic suspension bearing system under three controllers.

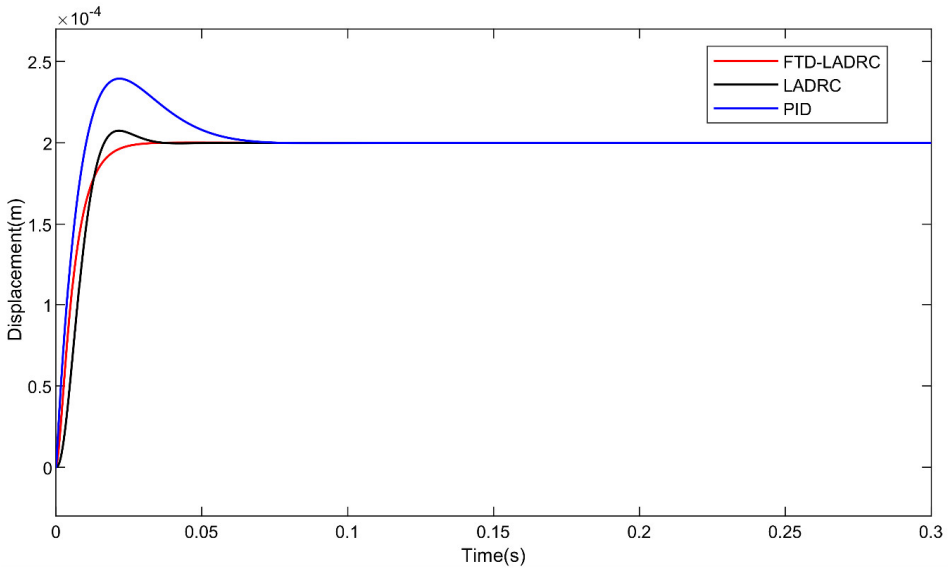

Figure 9. Step response curves of three controllers when ω_o of LADRC changes.

3) Load disturbance case

In the process of steady suspension of rotor, load mutation often occurs. In order to verify the ability of magnetic suspension bearing system to suppress load mutation, step disturbance is added in the simulation to verify the anti-disturbance effect of the three controllers. Displacement 0 was selected as the stable suspension position, and a 10 N step disturbance was added at 0.1 s. As shown in Figure 10, the maximum displacement offset of the rotor under PID control is 35 μm, and the equilibrium position is restored at 0.07 s. The rotor of maximum displacement offset and recovery time of LADRC are reduced by more than 50% compared with PID. However, the maximum displacement of the rotor controlled by the FTD-LADRC is very small, about 2 μm, and its anti-interference and rapidity are greatly improved.

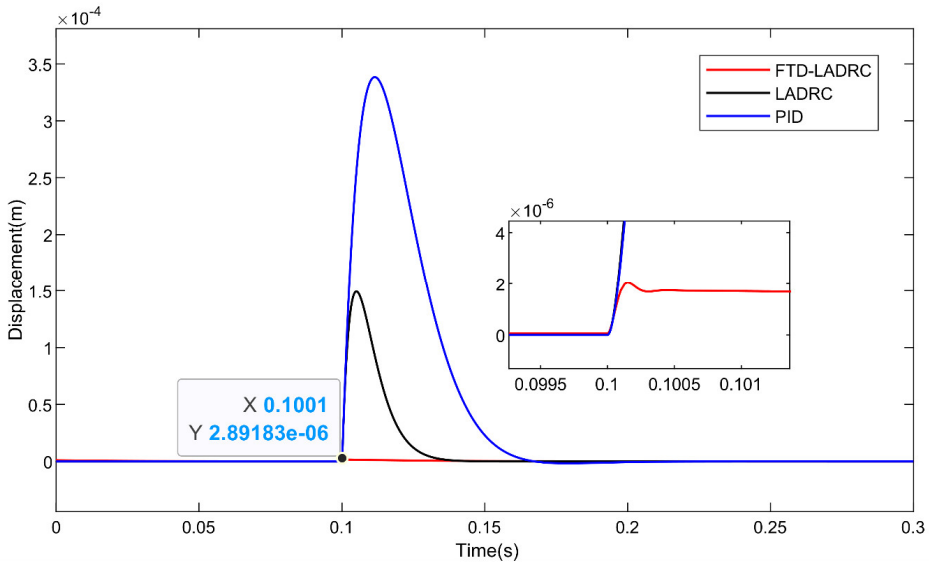

Figure 10. Simulation of step disturbance applied to magnetic bearing rotor control system.

4) Periodic square wave disturbance case

When the rotor is actually suspended, it may be subjected to a certain frequency of interference force. In order to verify the anti-interference of the control system under the action of periodic external force, a 100 N square wave with a period of 0.1 s was added to the simulation.

It can be seen from the simulation results that the maximum displacement fluctuation under PID control is 0.068 mm, and the maximum displacement fluctuation under LADRC control is 0.028 mm. The rotor displacement fluctuation using FTD-LADRC is 1.8×10^{-4} mm, and the square wave interference is greatly suppressed.

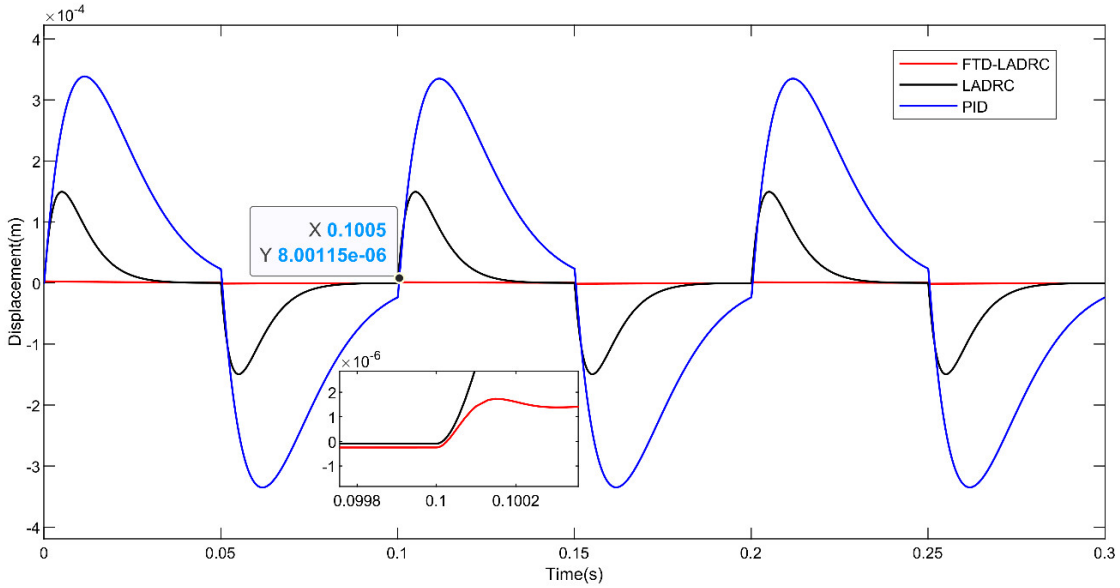

Figure 11. Simulation of square wave disturbance imposed by magnetic levitation rotor control system.

5) Noise interference case

Due to the complex engineering environment of the rotor, the mechanical structure part is in the environment of strong electricity and magnetic field, and there is some noise interference. Therefore, it is necessary to verify the anti-noise ability of the control system. White Gaussian noise with mean value of 0 and mean square deviation of 0.003 is added into the system. The simulation results are shown in Figure 12. The noise of the magnetic bearing system controlled by LADRC is obviously less than that controlled by PID. The filtering effect of FTD-LADRC is more obvious due to the addition of FTD.

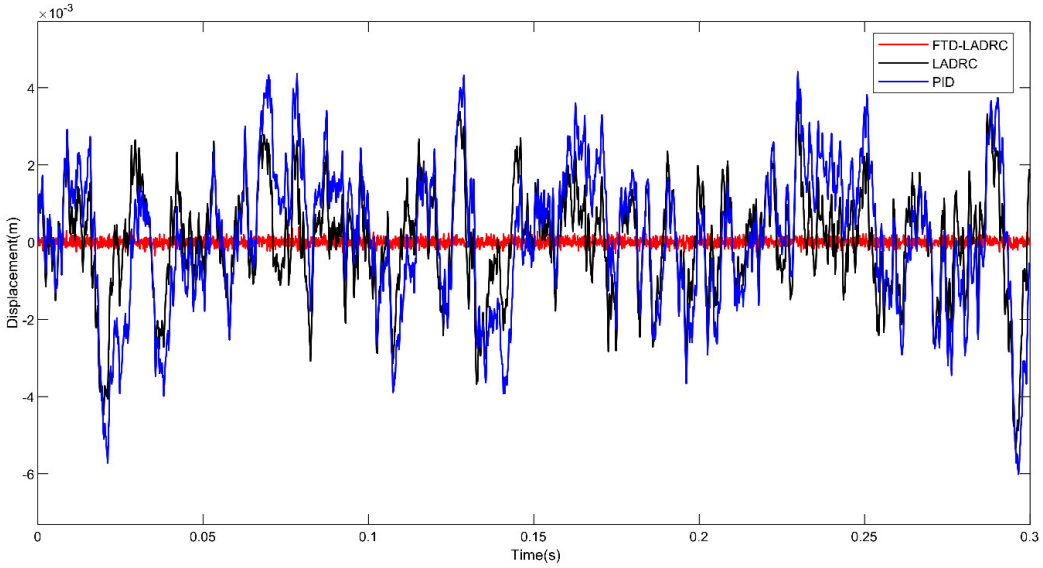

Figure 12. Simulation of noise interference imposed by magnetic levitation rotor control system.

5. Conclusions

In order to further improve the stability of the rotor of maglev turbomachinery system, this paper focuses on the improved linear active disturbance rejection control method against some uncertainties such as unknown mutation, time variation and load perturbation and so on. The electromagnetic bearing-rotor system of maglev turbomachinery is modeled, an improved linear active disturbance rejection control with fast tracking differentiator is proposed, and the method of PID, LADRC and FTD-LADRC are compared. The main contributions are concluded as follows:

1) Compared to the classic PID control, the LADRC can estimate the external disturbance of the magnetic suspension bearing system well, and compensate the estimated disturbance action in time. Thus, the magnetic suspension bearing system can better overcome the influence of external uncertainty disturbance.

2) The FTD can arrange the appropriate transition process according to the control objectives to avoid the oscillation or even instability caused by large overshoot of the bearing system during startup. Although the adjustable parameters of FTD-LADRC are increased compared with LADRC, the controller tuning has a certain rule, which can better suppress external disturbance, load mutation, and noise interference.

To sum up, the FTD-LADRC method magnetic levitation bearing system, which solves the problems of overshoot and vibration, has fast adjustment speed, strong robustness and anti-interference.

And the FTD-LADRC method can realize the stable suspension of the rotor of the magnetic levitation turbomachinery. The experimental research in this area will be further carried out in the future.

Acknowledgments

The authors would like to thank the referees for their comments and suggestions which helped to improve the manuscript. This work was supported by National Natural Science Foundation of China (61304036).

Conflict of interest

The authors declare no conflict of interest. The founding sponsors had no role in the design of the study; in the collection, analyses, or interpretation of data; in the writing of the manuscript, and in the decision to publish the results.

References

1. H. L. Sha, T. Y. Yu, Y. He, Z. H. Zhang, Rotor dynamics design and test of 700 kW magnetic levitation turbo blower, *Chin. J. Turbomach.*, **61** (2019), 45–47. https://doi.org/10.16492/j.fjjs.2019.06.0008
2. X. D. Guan, J. Zhou, C. W. Jin, Y. P. Xu, Disturbance suppression in active magnetic bearings with adaptive control and extended state observer, *Proc. Inst. Mech. Eng., Part I: J. Syst. Control Eng.*, **234** (2020), 272–284. https://doi.org/10.1177/0959651819849774
3. Z. W. Huang, J. M. Zhu, J. J. Shao, Z. X. Wei, J. W. Tang, Recurrent neural network based high-precision position compensation control of magnetic levitation system, *Sci. Rep.*, **12** (2022), 11435. https://doi.org/10.1038/s41598-022-15638-0
4. A. Hezzi, S. B. Elghali, Y. Bensalem, Z. B. Zhou, M. Benbouzid, M. N. Abdelkrim, ADRC-based robust and resilient control of a 5-phase PMSM driven electric vehicle, *Machines*, **8** (2020), 17. https://doi.org/10.3390/machines8020017
5. A. Winursito, G. N. P. Pratama, LQR state feedback controller with precompensator for magnetic levitation system, *J. Phys.: Conf. Ser.*, **2111** (2021), 012004. https://doi.org/ 10.1088/1742-6596/2111/1/012004
6. L. Zhang, L. W. Zhang, J. W. Yang, M. Gao, Y. H. Li, Application research of fuzzy PID control optimized by genetic algorithm in medium and low speed maglev train charger, *IEEE Access*, **9** (2021), 152131–152139. https://doi.org/ 10.1109/ACCESS.2021.3123727
7. J. Q. Han, Auto disturbances rejection controller and its applications, *Control Decis.*, **13** (1998), 19–23. https://doi.org/10.13195/j.cd.1998.01.19.hanjq.004
8. W. Zhan, J. Y. Su, G. J. Yang, Electrical line-shafting control for permanent magnet synchronous motors using active disturbance rejection control, *J. Phys.: Conf. Ser.*, **1884** (2021), 012036. https://doi.org/10.1088/1742-6596/1884/1/012036
9. Z. Q. Gao, Scaling and bandwidth-parameterization based controller tuning, in *Proceedings of American Control Conference*, **6** (2003), 4989–4996. https://doi.org/10.1109/ACC.2003.1242516
10. Y. L. Shi, C. Z. Hou, Design of improved nonlinear tracking, *Control Decis.*, **23** (2008), 647–650. https://doi.org/10.13195/j.cd.2008.06.49.shiyl.005

11. J. C. Ji, C. H. Hansen, Nonlinear oscillations of a rotor in active magnetic bearings, *J. Sound Vib.*, **240** (2001), 599–612. https://doi.org/10.1006/jsvi.2000.3257
12. L. L. Zhang, Vibration analysis and multi-state feedback control of maglev vehicle-guideway coupling system, *Electron. Res. Arch.*, **30** (2022), 3887–3901. https://doi.org/10.3934/era.2022198
13. J. C. Ji, Dynamics of a Jeffcott rotor-magnetic bearing system with time delays, *Int. J. Non-Linear Mech.*, **38** (2003), 1387–1401. https://doi.org/10.1016/S0020-7462(02)00078-1
14. J. C. Ji, C. H. Hansen, A. C. Zander, Nonlinear dynamics of magnetic bearing systems, *J. Intell. Mater. Syst. Struct.*, **19** (2008), 1471–1491. https://doi.org/10.1177/1045389X08088666
15. F. T. Wang, P. Dai, J. P. Wang, L. K. Niu, Vibration responses of the bearing-rotor-gear system with the misaligned rotor, *Machines*, **10** (2022), 267. https://doi.org/10.3390/machines10040267
16. N. Numanoy, J. Srisertpol, Vibration reduction of an overhung rotor supported by an active magnetic bearing using a decoupling control system, *Machines*, **7** (2019), 73. https://doi.org/10.3390/machines7040073
17. Y. H. Wang, X. Xiong, X. Hu, Vibration and stability analysis of a bearing–rotor system with transverse breathing crack and initial bending, *Machines*, **9** (2021), 79. https://doi.org/10.3390/machines9040079
18. Z. L. Xie, J. Jiao, K. Yang, T. He, R. G. Chen, W. D. Zhu, Experimental and numerical exploration on the nonlinear dynamic behaviors of a novel bearing lubricated by low viscosity lubricant, *Mech. Syst. Sig. Process.*, **182** (2023), 109349. https://doi.org/10.1016/j.ymssp.2022.109349
19. L. Y. Huang, N. Q. Hu, Y. Yang, L. Chen, J. H. Wen, G. J. Shen, Study on electromagnetic–dynamic coupled modeling method—detection by stator current of the induction motors with bearing faults, *Machines*, **10** (2022), 682. https://doi.org/10.3390/machines10080682
20. J. Wang, Y. F. Liu, Z. Y. Qin, L. Ma, F. L. Chu, Dynamic performance of a novel integral magnetorheological damper-rotor system, *Mech. Syst. Sig. Process.*, **172** (2022), 109004. https://doi.org/10.1016/j.ymssp.2022.109004
21. B. Xiang, H. Liu, Y. J. Yu, Gimbal effect of magnetically suspended flywheel with active deflection of Lorentz-force magnetic bearing, *Mech. Syst. Sig. Process.*, **173** (2022), 109081. https://doi.org/10.1016/j.ymssp.2022.109081
22. Z. J. Wang, T. Zhao, Adaptive-based linear active disturbance rejection attitude control for quadrotor with external disturbances, *Trans. Inst. Meas. Control*, **44** (2022), 286–298. https://doi.org/10.1177/01423312211031781
23. J. Q. Han, L. L. Yuan, The discrete form of tracking differentiator, *J. Syst. Sci. Math. Sci.*, **19** (1999), 268–273.
24. S. N. Wu, Z. L. Ping, Y. H. Ma, Research on DPCC control strategy of PMSM based on LESO, *J. Phys.: Conf. Ser.*, **2005** (2021), 012137. https://doi.org/10.1088/1742-6596/2005/1/012137
25. Y. T. Wang, W. Tan, W. Q. Cui, Tuning of linear active disturbance rejection controllers for second-order underdamped systems with time delay, *ISA Trans.*, **118** (2021), 83–93. https://doi.org/10.1016/j.isatra.2021.02.011
26. X. D. Sun, Z. J. Jin, L. Chen, Z. B. Yang, Disturbance rejection based on iterative learning control with extended state observer for a four-degree-of-freedom hybrid magnetic bearing system, *Mech. Syst. Signal Process.*, **153** (2021), 107465. https://doi.org/10.1016/j.ymssp.2020.107465

AIMS Press